

Carbon Suboxide in Astrophysical Ice Analogs

P. A. Gerakines¹ and M. H. Moore

Astrochemistry Branch, Code 691, NASA's Goddard Space Flight Center, Greenbelt, Maryland 20771

E-mail: gerakines@uab.edu

Received January 18, 2001; revised July 5, 2001

As suggested by W. T. Huntress *et al.* (1991, *Nature* 352, 316–318), carbon suboxide (C_3O_2) is a potential extended source of both the CO and atomic carbon emission observed in cometary comae. However, laboratory experiments on the formation and stability of C_3O_2 in space environments have not been published. In this work, we study solid C_3O_2 in ices representative of cometary nuclei as well as interstellar icy grain mantles, specifically addressing the issues of C_3O_2 formation and stability under exposure to energetic processing in the forms of proton irradiation and UV photolysis. The formation rate of C_3O_2 is measured in laboratory ices of pure CO and CO_2 and mixtures of these molecules with H_2O at 18 K. Destruction rates in H_2O -dominated mixtures appropriate to a cometary nucleus or interstellar icy grain mantle are also measured. Differences in rates between photolysis and irradiation experiments are observed and quantified. Mid-infrared spectra of C_3O_2 -containing mixtures are presented together with measurements of carbon suboxide's infrared band strengths and vapor pressures from 110 to 125 K. Implications are discussed for the existence of C_3O_2 under the energetic conditions found in astrophysical environments as well as the possibility for its detection in cometary and/or interstellar ices. © 2001 Elsevier Science (USA)

Key Words: ices; comets, composition; radiation chemistry; photochemistry; spectroscopy.

1. INTRODUCTION

Huntress *et al.* (1991) proposed carbon suboxide (C_3O_2) as a possible source of both the extended neutral atomic carbon and molecular carbon monoxide emission observed in the coma of Comet Halley (e.g., Festou *et al.* 1986, Woods *et al.* 1987, Eberhardt *et al.* 1987). C_3O_2 is a well-studied oxide of carbon, made up of two carbon monoxide groups linked to a carbon atom to form a linear structure: $O=C=C=O$. In the laboratory, it is widely used as a source of atomic carbon. As a gas it can be stored in a bulb at a pressure of a few mm Hg, but under conditions of standard temperature and pressure (300 K, 1 atm), C_3O_2 forms a yellow, red, or brown polymer. (The yellowish clouds on

Venus were once attributed to C_3O_2 polymer by Kuiper (1957), but Plummer and Carson (1970) later presented spectroscopic evidence proving this to be incorrect.) Suboxide polymers form when CO is processed (by electrolysis, irradiation, or photolysis) in the gas, liquid, or condensed phase (e.g., Lind 1928, Sugimoto *et al.* 1986, Briggs and Clay 1968, Haring *et al.* 1984). Studies of the electrical discharge of CO date back to Brodie (1873) who first showed that its decomposition products formed a reddish brown solid. If present on the surfaces of cometary nuclei, C_3O_2 polymers may contribute to their low geometric albedo, which is typically around 4% (as measured toward Comet Halley by, e.g., Sagdeev *et al.* (1986)).

Spectral features of monomeric C_3O_2 are unobservable in the gas phase of the interstellar medium or in cometary comae, because C_3O_2 is a linear, symmetric molecule with no dipole moment and hence no rotational transitions at submillimeter or radio wavelengths. It may be possible to detect cosmic C_3O_2 in the solid phase, however, since it forms a highly interactive crystalline matrix with a variety of absorption features throughout the mid-infrared region, e.g., Miller and Fateley (1964).

In this paper, we study C_3O_2 under conditions that more appropriately reflect the environments and compositions of cometary and interstellar ices in order to understand its formation and stability in an astrophysical context. Experimental results are presented for solid C_3O_2 formation and energetic processing in laboratory analogs of astrophysical ices (both cometary and interstellar) at low temperature, $T = 15$ –20 K. The laboratory system, sample preparation, and processing techniques are described in Section 2. Mid-IR spectra (5000 – 400 cm^{-1} ; 2 – $25\text{ }\mu\text{m}$) for C_3O_2 diluted in different ice matrices at 18 K are presented in Section 3, along with calculations of the strengths (“*A* values”) of the C_3O_2 IR absorption features and C_3O_2 vapor pressures from 110 to 125 K. The formation of C_3O_2 resulting from energetic processing of CO and CO_2 in pure form and in mixtures with H_2O by both proton irradiation and UV photolysis² is measured in Section 4, together with destruction rates in H_2O -dominated matrices. Implications for the existence of C_3O_2 in

¹ Current address: Astro- and Solar-System Physics Program, Department of Physics, University of Alabama at Birmingham, 1300 University Boulevard, Birmingham, AL 35294-1170.

² Hereafter, to clearly distinguish one from the other, we refer to energetic processing by high-energy particles such as protons as “irradiation” and to processing by ultraviolet light as “photolysis.”

the ices found within interstellar clouds and in cometary nuclei and the possibilities for its detection in those environments are discussed in Section 5.

2. EXPERIMENTAL

Hudson and Moore (1995) have described the laboratory setup at NASA's Goddard Space Flight Center in detail. In summary, gases are prepared inside a vacuum manifold and vapor-condensed onto a cold (15–20 K) aluminum mirror suspended inside a stainless-steel high-vacuum chamber ($P \approx 10^{-7}$ mm Hg). Mixing ratios in the resultant ice are determined from the partial pressures inside the gas-filled manifold before condensation. Actual ratios in the resulting ice samples may vary slightly from these values because of effects of depositing through a narrow tube, (see, e.g., the discussion in Gerakines *et al.* (1995)), but any differences should not exceed a factor of 2. Since the differences in mixing ratios between the ice mixtures studied are large (100:1 or 10:1 matrix:suboxide ices are compared to those with ratios of about 1:1), the qualitative differences between the 100:1 or 10:1 ices and the 1:1 ices should not be significantly affected (such as those observed in the IR spectra; see Section 3). The quantitative measurements made do not depend critically upon the mixing ratio, but on the general nature of the ice (such as the rates of C_3O_2 formation in various pure ices and in an H_2O -dominated ice; see Section 3).

The temperature of the mirror may be controlled up to room temperature. IR spectra (with a spectral range of 5000 to 400 cm^{-1} and resolutions from 1 to 4 cm^{-1}) are taken by diverting the beam of an FTIR spectrometer (Mattson Instruments) toward the ice-covered mirror, where it passes through the ice before and after reflection at the ice-mirror interface. Ices are processed by turning the mirror to face either a beam of 0.8-MeV protons generated by a Van de Graaff accelerator or UV photons from a microwave-discharged hydrogen flow lamp. Photons from the UV lamp, limited by the LiF window between the H_2 discharge and the vacuum system, fall in the wavelength range of 110–250 nm. The total UV photon flux at the ice sample was determined to be approximately 8.6×10^{13} photons $cm^{-2} s^{-1}$ by Gerakines *et al.* (2000), who describe this measurement in detail and outline the methods by which both irradiation and photolysis energy doses are calculated.

The C_3O_2 used in these experiments was generated by the method described by Miller and Fateley (1964). In summary, a mixture of $CH_2(COOH)_2$ (malonic acid) and P_2O_5 (phosphorus pentoxide) in approximate 10:1 weight ratio was heated to 410–420 K for 1 h. The gases produced (H_2O , CO_2 , C_3O_2 , and CH_3COOH) were collected at 77 K using liquid N_2 . The CO_2 was removed from the sample by replacing the liquid N_2 with a liquid-solid bath of ethanol at 156 K and pumping on the sample for 1 h. To remove the C_3O_2 from the remaining sample, the ethanol was replaced by a liquid-solid chloroform ($CHCl_3$) bath at 210 K and the evaporated C_3O_2 transferred to a bulb cooled with liquid N_2 . We produced about 5 torr-liters of C_3O_2

(0.3 mmol) from approximately 5 g (50 mmol) of malonic acid using this method. Over the course of several days, the C_3O_2 stored in the glass bulb at about 15 torr was seen to decompose (through spectroscopy of the contents of the gas bulb) into CO_2 (approximately 1 torr of CO_2 per week of storage). This CO_2 gas was removed before each experiment using a liquid-solid bath of ethanol as described above.

Reagents used and their purities are as follows: H_2O (triply distilled, with a resistance greater than 10^7 ohm cm), CO (gas, Matheson, 99.99%), CO_2 (gas, Matheson, 99.995%), N_2 (gas, Air Products, 99.9995%), malonic acid, $CH_2(COOH)_2$ (Aldrich, 99% purity), and phosphorous pentoxide, P_2O_5 (Aldrich, 98% purity).

3. RESULTS

Infrared Spectral Properties

The mid-IR spectrum (5000–400 cm^{-1} or 2–25 μm) of pure C_3O_2 at 18 K is shown in Fig. 1 at a resolution of 4 cm^{-1} . Peak positions and vibrational mode assignments are listed in Table I. They are in close agreement with those of pure C_3O_2 at 100 K reported by Miller and Fateley (1964) and matrix-isolated C_3O_2 in Ar (Ames *et al.* 1963, Miller and Fateley 1964, Smith and Leroi 1966).

The strongest absorption in the IR spectrum of C_3O_2 (Fig. 1) is its ν_3 anti-symmetric stretching vibration that falls near 2200 cm^{-1} (4.5 μm). Using standard methods (of condensing a sample to a known thickness and assuming a mass density of 1 g cm^{-3}), we used the area under this feature to calculate its integrated absorbance (a.k.a. “band strength” or “A value”) of $A(C_3O_2, \nu_3) = (1.3 \pm 0.2) \times 10^{-16}$ cm molecule $^{-1}$. (Since we have assumed a mass density equal to that of water in our

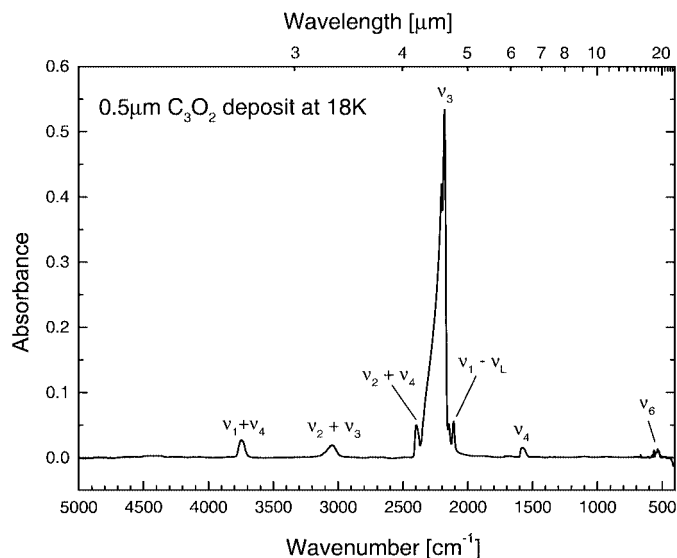


FIG. 1. Mid-IR spectrum (5000–400 cm^{-1} , 2–25 μm) of pure C_3O_2 at 18 K. Band assignments are taken from Miller and Fateley (1964) and Smith and Leroi (1966).

TABLE I
Observed Mid-IR Spectrum of Pure C₃O₂ at 18 K

Position (cm ⁻¹)	Assignment ^a	Band strength, A (10 ⁻¹⁸ cm molecule ⁻¹)	Comment
3744 m	$\nu_1 + \nu_4$	3.8 ± 0.6	
3043 m	$\nu_2 + \nu_3$	6 ± 1	
2756 vw	$\nu_1 + \nu_6$	—	
2666 vw	$\nu_4 + \nu_5$	—	
2396 m	$\nu_2 + \nu_4$	8 ± 4	
2200, 2177 vs	ν_3	130 ± 20	CCO asym. str
2109 m	$\nu_1 - \nu_L$	—	
1581 m	ν_4	5 ± 3	CC asym. str
~540 w	ν_6	1.4 ± 0.3	bend

^aAssignments taken from Miller and Fateley (1964) and Smith and Leroi (1966).

calculations, the “true” magnitude of *A* will scale inversely with the actual mass density of the C₃O₂ ice sample, which is unknown. The precision of our measurement is unaffected by the value of mass density.) This value of *A* is about 15–20 times stronger than any of the other observed C₃O₂ mid-IR features (see Table I). It is comparable to that of the ν_3 stretching vibration of H₂O at 3240 cm⁻¹ (3.1 μm), which has a band strength of about 1.6 × 10⁻¹⁶ cm molecule⁻¹ (Hagen *et al.* 1983). The strength of the stretching vibration of CO near 2140 cm⁻¹ (4.67 μm) is 10 times lower than that of C₃O₂, at 1.1 × 10⁻¹⁷ cm molecule⁻¹ (Jiang *et al.* 1975).

Pure C₃O₂ sublimates during warming in our system near 120 K. Evidence for a possible phase change (based upon changes in two of the overtone features) is seen between 50 and 75 K. McDougall and Kilpatrick (1965), who measured various thermodynamic properties of C₃O₂ over this temperature range, did not find evidence for a solid–solid phase transition, but the IR spectroscopic data (Fig. 2) do suggest a structural change in the C₃O₂ ice. Figure 2 contains spectra of the $\nu_1 + \nu_4$ (4000–3500 cm⁻¹), ν_3 (2500–2000 cm⁻¹), and ν_4 (1700–1450 cm⁻¹) C₃O₂ absorption features at 22, 50, 75, and 100 K. A gradual change is apparent in the $\nu_1 + \nu_4$ and ν_4 features from 50 to 100 K, indicated by shifts in peak position, decreases in width, and increases in peak absorbance. The ν_3 feature itself does not exhibit any significant changes over this temperature range, although the widths and peak absorbance values for its subpeaks near 2400 and 2100 cm⁻¹ do show change.

The C₃O₂ ν_3 stretching feature’s position, width, and profile are all sensitive to the dilution of C₃O₂ in an ice matrix. Figure 3 contains the 2500–2000 cm⁻¹ (4–5 μm) spectra of pure C₃O₂ (from Fig. 1), and C₃O₂ diluted in matrices of N₂, CO₂, H₂O, and CO. Dilution factors are 100 : 1 (matrix : suboxide) except in the H₂O-dominated ice, where it is 10 : 1. The ν_3 peak position (marked with asterisks in Fig. 3) varies by more than 50 cm⁻¹ as a result of the change in the ice matrix, from 2253 cm⁻¹ in an N₂ matrix to 2200 cm⁻¹ in the pure C₃O₂ sample (there is also a subpeak that falls at 2178 cm⁻¹ in the pure C₃O₂ sample). The width and profile of the feature also vary depending on the

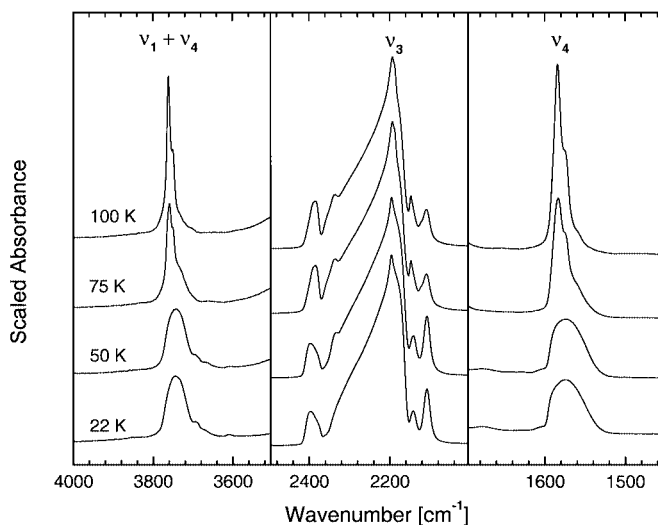


FIG. 2. Three features of pure C₃O₂: the $\nu_1 + \nu_4$ feature from 4000 to 3500 cm⁻¹ (left box), the ν_3 feature from 2500 to 2000 cm⁻¹ (middle box), and the ν_4 feature from 1700 to 1450 cm⁻¹ (right box) at temperatures of 22, 50, 75, and 100 K (from bottom to top).

matrix. It is sharp and singly peaked in matrices of N₂, CO, and CO₂ (FWHM = 8–14 cm⁻¹). It takes on a broad Gaussian profile when diluted in an H₂O matrix (FWHM = 90 cm⁻¹), since the polar nature of the H₂O ice creates a high degree of molecular

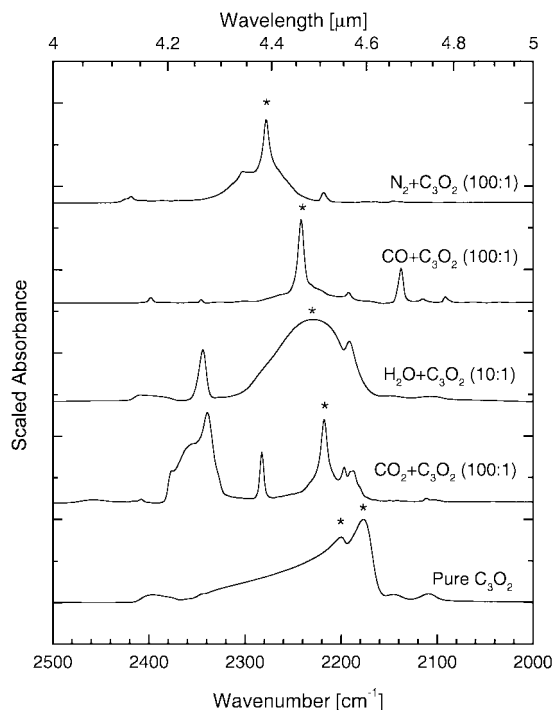


FIG. 3. Mid-IR spectra of the C₃O₂ ν_3 asymmetric stretching fundamental from 2500 to 2000 cm⁻¹ (4 to 5 μm) for C₃O₂ in various ice matrices at 18 K. From top to bottom: N₂ + C₃O₂ (100 : 1), CO + C₃O₂ (100 : 1), H₂O + C₃O₂ (10 : 1), CO₂ + C₃O₂ (100 : 1), and pure C₃O₂. The peak position of the ν_3 feature is marked with an asterisk in each case.

TABLE II
Position and Width (FWHM) of the C_3O_2 ν_3 Stretching Feature in Selected Mixtures at 18 K

Ice mixture	Position (cm^{-1})	FWHM (cm^{-1})
Pure C_3O_2	2200, 2178	67
$CO_2 + C_3O_2$ (100:1)	2217	11
$H_2O + C_3O_2$ (10:1)	2233	90
$CO + C_3O_2$ (100:1)	2242	8
$N_2 + C_3O_2$ (100:1)	2253	14

interaction. In a pure C_3O_2 sample, the stretching feature is broad (FWHM = 67 cm^{-1}), double-peaked (peaks falling at 2200 and 2178 cm^{-1}), and asymmetric, with a long-wavelength wing that extends to about 2350 cm^{-1} ($4.26\text{ }\mu\text{m}$). Within the $2200\text{--}2300\text{ cm}^{-1}$ region, there is also a notable amount of substructure to the C_3O_2 feature, possibly because of C_3O_2 dimers, trimers, or higher n -mers. Table II summarizes the ν_3 peak's position and FWHM for pure C_3O_2 and C_3O_2 in several different ice matrices at 18 K.

Vapor Pressure

The vapor pressure (P_{vap}) of C_3O_2 was measured at 110, 115, 120, and 125 K by observing the sublimation rate (dN/dt , in $cm^{-2}\text{ s}^{-1}$) for about 30 minutes at each temperature and using the relation

$$P_{vap} = (dN/dt) \times (2\pi m kT)^{1/2}, \quad (1)$$

where m is the molecular mass of C_3O_2 (68 amu). The term dN/dt was determined at each temperature of interest by holding the sample at that temperature and measuring the linear change in N versus time. The term N was measured at various time steps by integrating the area underneath the C_3O_2 ν_3 feature and dividing by its band strength (the measurement of which is described previously in this section). Calculated values of P_{vap} are listed in Table III. At 110 K, pure C_3O_2 has a vapor pressure of 1.2×10^{-8} mm Hg, but at 125 K, it has risen sharply to 5.8×10^{-6} mm Hg (C_3O_2 vapor pressures for $T = 160\text{--}248$ K have been measured by McDougall and Kilpatrick (1965)). In comparison, the vapor pressure of H_2O ice, which depends on its crystalline state, can vary from $\sim 10^{-7}$ to $\sim 10^{-6}$ mm Hg at 125 K (Kouchi 1987).

TABLE III
Vapor Pressure of C_3O_2

T (K)	P (10^{-7} mm Hg)
110	0.12 ± 0.01
115	0.90 ± 0.13
120	2.1 ± 0.1
125	58 ± 1

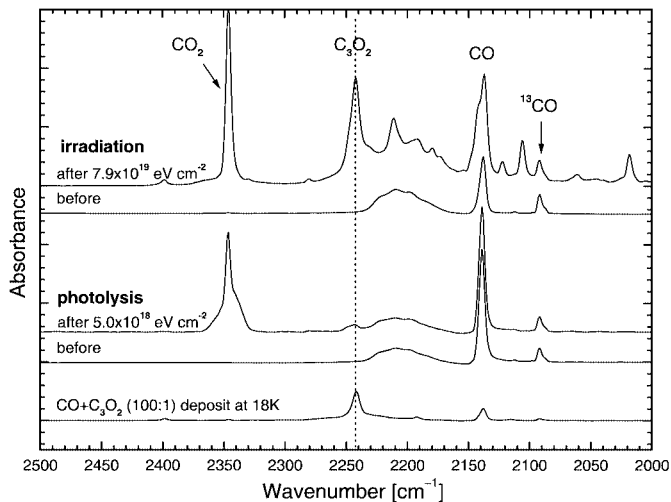


FIG. 4. Spectra of pure CO from 2500 to 2000 cm^{-1} (4 to $5\text{ }\mu\text{m}$) before and after processing at 18 K by proton irradiation (to a dose of $7.9 \times 10^{19}\text{ eV cm}^{-2}$) and UV photolysis (to a dose of $5.0 \times 10^{18}\text{ eV cm}^{-2}$). The spectrum of $CO + C_3O_2$ (100:1) at 18 K (bottom) is shown for comparison. The dotted line indicates the peak position of the C_3O_2 stretching feature in the $CO + C_3O_2$ (100:1) ice.

Suboxide Formation and Energetic Processing

As noted above, C_3O_2 and/or C_3O_2 polymers are known to form from pure CO energetically processed in its gas (Sugimoto *et al.* 1986), liquid (Briggs and Clay 1968), or solid phases (Haring *et al.* 1984). Here, we measure the production rates of C_3O_2 from pure, solid CO at 18 K as processed by irradiation and by photolysis. This is the first direct comparison of pure CO irradiation and photolysis known to us. The IR spectrum of the pure CO sample at 18 K before and after processing is shown in Fig. 4 for each case. The spectrum of the $CO + C_3O_2$ 100:1 sample from Fig. 3 is presented for comparison; note that the broad feature near 2210 cm^{-1} present in each of the pure CO spectra is not due to an impurity in the CO ice, but it is a weak absorption of CO itself exaggerated by the scale of the figure and is due to a combination of the CO lattice mode and fundamental stretching mode; see, e.g., Ewing and Pimentel (1961) or Pipes *et al.* (1978) for identifications of this feature. A forest of absorptions appears in the $2500\text{--}2000\text{ cm}^{-1}$ ($4\text{--}5\text{ }\mu\text{m}$) range after irradiation processing. The major products formed in these experiments include CO_2 (peak near 2340 cm^{-1}), C_3O_2 (2242 cm^{-1}), and C_2O (1990 cm^{-1} ; not shown in Fig. 4). Other, less abundant species such as C_3O , and C_4O are also likely sources of the other, unidentified peaks shown in Fig. 4 (irradiation case).

The abundances of the major products are plotted against the total applied energy dose in Fig. 5 for both irradiation and photolysis experiments. Formation yields have been measured from the slopes of the linear parts of the curves and are listed in Table IV, along with yields calculated from other ice experiments described below. Since the intrinsic band strength of C_2O is unknown, an estimate of its abundance was made assuming a value of $A = 1 \times 10^{-17}\text{ cm molecule}^{-1}$. Yields of CO_2 were

TABLE IV
 Yields, G , in Processing Experiments (in Units of Molecules per 100 eV Absorbed)

Initial ice	$G(\text{CO})$		$G(\text{CO}_2)$		$G(\text{C}_3\text{O}_2)$	
	p+	UV	p+	UV	p+	UV
CO	—	—	0.25(4)	0.9(2)	0.24(4)	0.014(1)
CO ₂	1.1(1)	8.1(3)	—	—	<0.001	<0.001
C ₃ O ₂	0.68(4)	1.1(1)	0.12(2)	0.074(4)	-4.3(4)	-6.5(4)
H ₂ O + C ₃ O ₂ (10 : 1)	0.063(8)	0.045(5)	0.019(4)	0.13(1)	-0.13(1)	-0.47(9)

Note. Numbers in parentheses represent uncertainty in final digit (e.g., “0.25(4)” = “0.25 ± 0.04”). Negative values indicate yields of destruction.

0.25 ± 0.04 molecules per 100 eV absorbed for irradiation and 0.9 ± 0.2 for photolysis, differing by a factor of about 3.6. Briggs and Clay (1968) reported a value of $G(\text{CO}_2) = 0.24 \pm 0.01$ molecules per 100 eV for the gamma radiolysis of liquid CO at 77 K.

It is clear from Figs. 4 and 5 that C₃O₂ is much more effectively produced by irradiation than by photolysis. The measured C₃O₂ yields are 0.24 ± 0.04 for irradiation and 0.014 ± 0.001 for photolysis (differing by a factor of 17). This is the first time a significant difference has been reported in any direct comparison of these two processing techniques. The differences in both measurements of the CO₂ and C₃O₂ yields are most likely linked to the strength of the CO bond, whose dissociation energy is 11.1 eV. While 0.8-MeV protons may easily break this bond directly, e.g.,

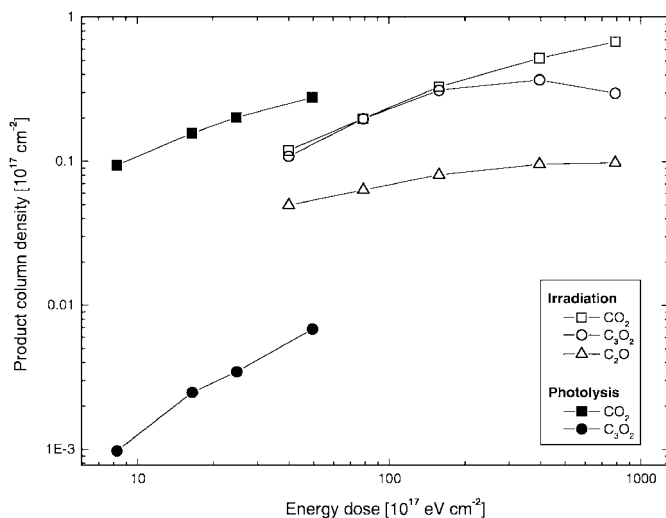
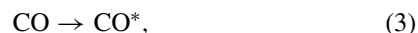


FIG. 5. Column density (10^{17} cm^{-2}) versus energy dose ($10^{17} \text{ eV cm}^{-2}$) for the products of pure CO processing at 18 K by both proton irradiation (open symbols) and UV photolysis (filled symbols). Squares represent CO₂, circles C₃O₂, and triangles C₂O (irradiation case only; C₂O abundance assumes $A = 1 \times 10^{17} \text{ cm molecule}^{-1}$).

6 to 10 eV photons cannot.³ Photolysis of CO proceeds through its indirect dissociation, a two-step process involving first the electronic excitation of one CO molecule (requires $E > 8.4 \text{ eV}$) and its subsequent reaction with another to form CO₂ and a carbon atom,



(Okabe 1978). Therefore, the formation of carbon chains and suboxides (C_n, C_nO, C_nO₂) is more effective in the irradiation case, whereas photolysis tends to form CO₂ before other carbon oxides.

C₃O₂ may also be a product to consider for CO₂ ice processing. In fact, C₃O₂ has been identified as a minor product in previous CO₂ processing studies with CO, CO₃, and O₃ in much higher abundances (e.g., Gerakines *et al.* 1996; Brucato *et al.* 1997). However, we find no indication of suboxide in the processed pure CO₂ ices studied here. Figure 6 contains IR spectra of the CO₂ ices in our processing experiments. Indeed, features due to CO (2139 cm⁻¹) and CO₃ (2046 cm⁻¹) appear strongly in our spectra (along with O₃ at 1045 cm⁻¹ and CO₃ at 1879 cm⁻¹; not shown in Fig. 6), but the C₃O₂ signal is not present. However, the feature of C₂O is found at 1991 cm⁻¹ (although weak). We place upper limits on the C₃O₂ yields of $G < 0.001 \text{ molecules } (100 \text{ eV})^{-1}$ in both irradiation and photolysis cases (Table IV), based on the noise levels in our laboratory spectra. Yields of CO were measured at $1.1 \pm 0.1 \text{ molecules } (100 \text{ eV})^{-1}$ for irradiation and 8.1 ± 0.3 for photolysis (see Table IV). The origin of this difference in formation yields may be that the CO produced from the parent CO₂ molecules is more easily destroyed by the irradiation (as indicated in the pure CO experiments described previously) and thus displays a lower net yield of formation.

³ While the end results will no doubt be quite different, the initiation of nitrogen chemistry in astrophysical ices should show a similar disparity between the processes of irradiation and photolysis, given that N₂, a molecule that is isoelectronic with CO, possesses a similarly high dissociation energy of 9.8 eV.

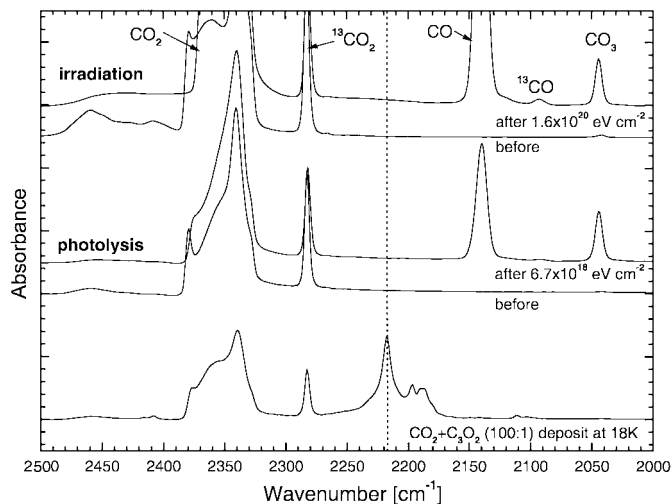


FIG. 6. Spectra of pure CO_2 from 2500 to 2000 cm^{-1} (4 to 5 μm) before and after processing by proton irradiation (to a dose of $1.6 \times 10^{20} \text{ eV cm}^{-2}$) and UV photolysis (to a dose of $6.7 \times 10^{18} \text{ eV cm}^{-2}$). The spectrum of $\text{CO}_2 + \text{C}_3\text{O}_2$ (100: 1) at 18 K (bottom) is shown for comparison. The dotted line indicates the peak position of the C_3O_2 stretching feature in the $\text{CO}_2 + \text{C}_3\text{O}_2$ (100: 1) ice.

We have also studied the processing of pure C_3O_2 samples at 18 K. Spectra are given in Fig. 7. The major products observed in both irradiation and photolysis experiments were CO (at 2138 cm^{-1}), CO_2 (at 2345 cm^{-1}), CO_3 (at 2056 cm^{-1}), and C_2O (at 1994 cm^{-1}). Other weaker features observed near 1948 and 1899 cm^{-1} in the irradiation experiment are suggestive of longer carbon chains (e.g., Kurtz and Huffman 1990, Kranze *et al.* 1996). Yields measured in the irradiation experiment were $G(\text{CO}) = 0.68 \pm 0.04$, $G(\text{CO}_2) = 0.12 \pm 0.02$, and $G(-\text{C}_3\text{O}_2) = 4.3 \pm 0.4$. Yields in the photolysis experi-

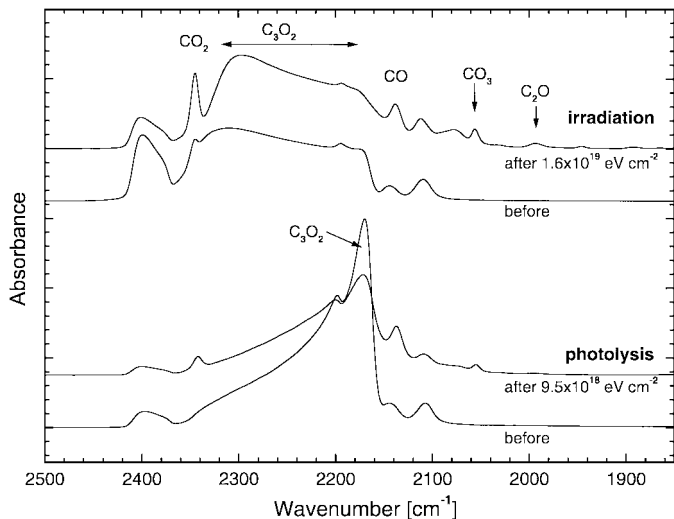


FIG. 7. Spectra of pure C_3O_2 at 18 K from 2500 to 1850 cm^{-1} (4 to 5.4 μm) before and after processing by proton irradiation (thickness of 2.1 μm , irradiated to a dose of $1.6 \times 10^{19} \text{ eV cm}^{-2}$) and UV photolysis (thickness of 0.52 μm ; photolyzed to a dose of $9.5 \times 10^{18} \text{ eV cm}^{-2}$).

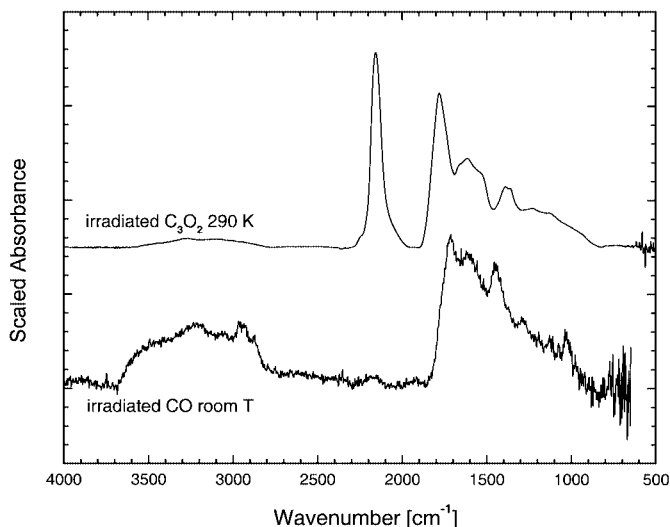


FIG. 8. Spectra of irradiated C_3O_2 warmed to 290 K (top) and irradiated CO after warming to room temperature (bottom).

ment were $G(\text{CO}) = 1.1 \pm 0.1$, $G(\text{CO}_2) = 0.074 \pm 0.004$, and $G(-\text{C}_3\text{O}_2) = 6.5 \pm 0.4$. In each case, the suboxide destruction yield is much greater than the combined CO and CO_2 formation yields, suggesting the abundant formation of unidentified products such as C_3O_2 polymers.

CO and CO_2 are released during warming of the irradiated pure C_3O_2 sample. A residue remains at 290 K, and its spectrum is shown in Fig. 8. The spectrum of the room-temperature residue of irradiated CO, which was obtained with an FTIR microscope, is shown for comparison. The two spectra show some weak similarities, and the relative strengths of specific features vary from one to the other. The major peaks in the IR spectrum of the C_3O_2 residue (with possible functional group assignments based on their peak wavenumber) fall at 2156 (CO groups), 1781 (C=O bonds), 1617 (C=C bonds), and 1388/1361 ($\text{O}=\text{C}-\text{O}$ groups). Weak absorption features also appear in the 3600–2850 cm^{-1} region, indicative of cyclic carbon structures; these features may imply the presence of C_3O_2 thermal polymer, as its structure is likely a polycyclic unsaturated lactone as described in Kybett *et al.* (1965) and the references therein. The residue of irradiated CO has a much weaker feature near 2160 cm^{-1} , and strong peaks at 1712, 1614, 1449, 1288, and 1031 cm^{-1} . Absorptions in the 3600–2850 cm^{-1} region are much stronger in this case. The color of the CO residue is dark reddish brown, and further characterizations in the UV and visible wavelength regions are in progress.

Since the ice environments of comets and interstellar ices are typically thought to be H_2O -dominated, the formation and destruction of C_3O_2 should be considered in ice samples where CO, CO_2 , and C_3O_2 have been diluted in H_2O . Work already present in the literature has shown that the major products of $\text{H}_2\text{O} + \text{CO}$ processing are CO_2 , HCO, H_2CO , and CH_3OH (photolysis: Sandford *et al.* 1988; irradiation: Hudson and Moore 1999). No detection of C_3O_2 has been noted. Previous studies

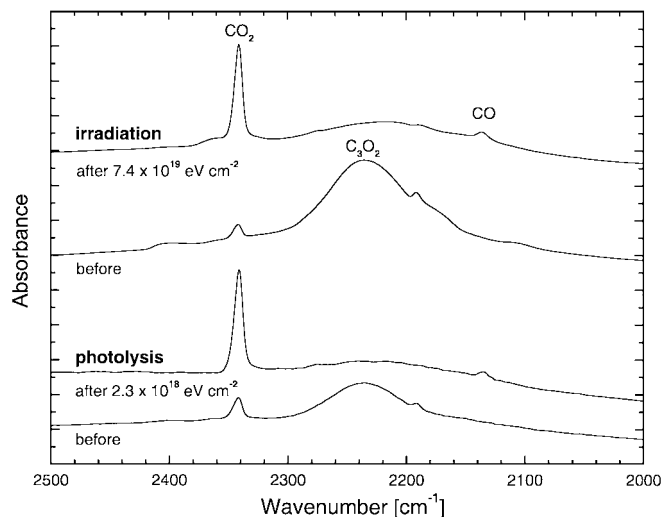


FIG. 9. Spectra of $\text{H}_2\text{O} + \text{C}_3\text{O}_2$ (10 : 1) at 18 K from 2500 to 2000 cm^{-1} (4 to 5 μm) before and after processing by proton irradiation (to a dose of $7.4 \times 10^{19} \text{ eV cm}^{-2}$) and UV photolysis (to a dose of $2.3 \times 10^{18} \text{ eV cm}^{-2}$).

of $\text{H}_2\text{O} + \text{CO}_2$ ices have shown that the major products of processing are CO, HCO, and H_2CO_3 (photolysis and irradiation: Gerakines *et al.* 2000), and, again, no detection of C_3O_2 was noted.

We have studied the processing of $\text{H}_2\text{O} + \text{C}_3\text{O}_2$ ice at low temperature. The $\text{H}_2\text{O} + \text{C}_3\text{O}_2$ (10 : 1) ice sample's spectrum before and after processing is shown in Fig. 9. The two major products of both irradiation and photolysis were found to be CO and CO_2 . Product column densities in the sample are shown in Fig. 10 as a function of absorbed energy dose. In the irradiation experiment, these species initially formed with yields of $G(\text{CO}) = 0.063 \pm 0.008$ and $G(\text{CO}_2) = 0.019 \pm 0.004$ (to a dose of $3 \times$

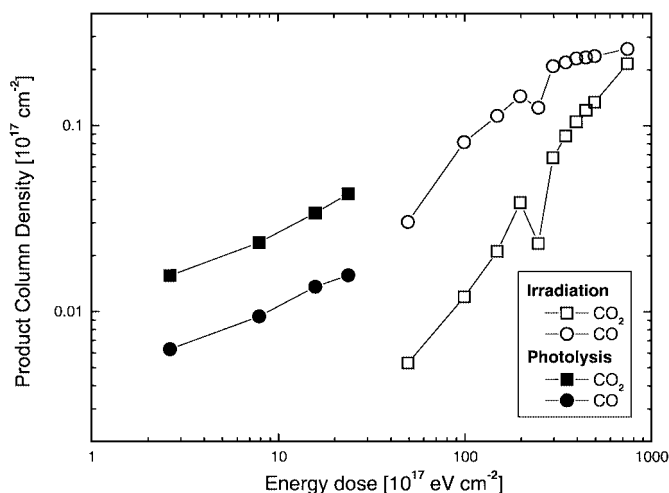


FIG. 10. Column density (10^{17} cm^{-2}) versus energy dose ($10^{17} \text{ eV cm}^{-2}$) for the products of $\text{H}_2\text{O} + \text{C}_3\text{O}_2$ (10 : 1) ice processing at 18 K by both proton irradiation (open symbols) and UV photolysis (filled symbols). Squares represent CO_2 , and circles CO.

$10^{19} \text{ eV cm}^{-2}$, see Fig. 10). Yields dropped at higher doses. The C_3O_2 was destroyed by irradiation with a destruction yield of $G(-\text{C}_3\text{O}_2) = 0.13 \pm 0.01$ to a dose of $3 \times 10^{19} \text{ eV cm}^{-2}$. In the photolysis experiment, where the total energy dose was $2.4 \times 10^{18} \text{ eV cm}^{-2}$, only linear production and destruction rates were apparent, and we measured yields of $G(\text{CO}_2) = 0.13 \pm 0.01$, $G(\text{CO}) = 0.045 \pm 0.005$, and $G(-\text{C}_3\text{O}_2) = 0.47 \pm 0.09$ (see Fig. 10).

4. DISCUSSION AND IMPLICATIONS

We have found that C_3O_2 has a mid-IR spectrum that is sensitive to the effects of dilution in a molecular matrix. The differences in the ν_3 peak's position between different ice matrices at low temperature are quite large. The extreme values of the peak position for the ν_3 C_3O_2 features are 2253 cm^{-1} in an N_2 -dominated ice at 18 K and 2178 cm^{-1} in a pure C_3O_2 ice at 18 K, with values for ices dominated by CO, CO_2 , and H_2O falling in between. The width of the ν_3 feature also varies greatly, from only 8 cm^{-1} in a CO-dominated ice at 18 K to 90 cm^{-1} in one that is H_2O -dominated as 18 K. Hence, the detection of this absorption feature in either the ISM or in planetary ices could lead to highly accurate determinations of the overall ice environment.

However, solid-phase C_3O_2 has not been positively identified in recent mid-infrared observations conducted by the Infrared Space Observatory (ISO). Figure 11 compares two ISO short-wavelength spectrometer (SWS) observations of high-mass protostars, W33A and NGC 7538 IRS9, to laboratory spectra of $\text{H}_2\text{O} + \text{C}_3\text{O}_2$ (10 : 1) and $\text{CO} + \text{C}_3\text{O}_2$ (100 : 1) at 18 K. Although small features do seem to exist in the spectral region near the expected position of the C_3O_2 ν_3 feature, these are likely well within the noise of the observed data. The observations of W33A

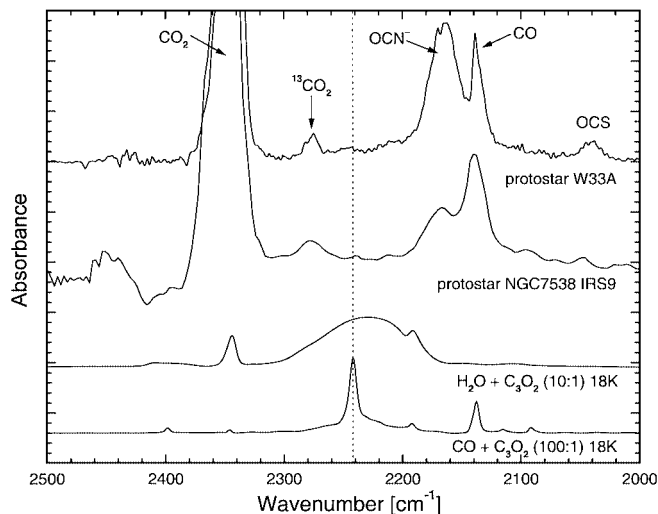


FIG. 11. ISO-SWS spectra of the protostars W33A (Gibb *et al.* 2000) and NGC 7538 IRS9 (Whittet *et al.* 1996) in the region of the C_3O_2 ν_3 stretching feature. The dotted line indicates the position (2242 cm^{-1}) of the C_3O_2 ν_3 stretching feature in the $\text{CO} + \text{C}_3\text{O}_2$ (100 : 1) ice sample.

(Gibb *et al.* 2000) were made at a spectral resolution of $\lambda/\Delta\lambda = 1500$, while those of NGC 7538 IRS9 (Whittet *et al.* 1996) have a lower resolution of $\lambda/\Delta\lambda = 500$. Upper limits on the C_3O_2 column density in these observations, based on the level of the noise between 2220 and 2250 cm^{-1} , are about $5 \times 10^{15} cm^{-2}$ for W33A (0.05% of H_2O) and $1 \times 10^{15} cm^{-2}$ for NGC 7538 IRS9; 0.01% H_2O ; H_2O column densities in these lines of sight may be found in Gibb *et al.* (2000). Other molecules such as N_2O also have absorption features in the 2200–2300 cm^{-1} region, and, if present, would lower this limit even further (N_2O has an absorption that falls at about 2235 cm^{-1} ; see e.g., Eلسila *et al.* 1997). This dearth of C_3O_2 comes despite the relatively high abundance of solid CO and CO_2 present in the sampled protostellar environments: the total amount of solid CO ranges from 2 to 15% of the H_2O ice column density (Gibb *et al.* 2000), and CO_2 from about 12 to 22% (Gerakines *et al.* 1999). Most other ice components are found at the 1% level relative to H_2O .

We have shown that C_3O_2 forms efficiently in pure CO ice samples when processed by irradiation with a yield of about 0.25 molecules per 100 eV absorbed. The yield of C_3O_2 by photolysis in similarly prepared CO ices is about 20 times smaller. However, it is not formed in significant abundances from pure CO_2 ice or from mixtures dominated by H_2O . Since interstellar ices toward massive protostars are largely composed of $H_2O + CO_2 + CH_3OH$ in the ratio of approximately 100 : 20 : 10 (Gerakines *et al.* 1999; Dartois *et al.* 1999; Gibb *et al.* 2000), it may not be surprising to note that C_3O_2 is not found there.

This may not be the final verdict for interstellar solid C_3O_2 , however, since an important observational bias exists in the ISO dataset because of the sensitivity limits of its instruments. The majority of sources observed were highly constrained to those bright in the mid infrared and, in the case of ice detections, almost entirely high-mass protostars. Detailed observations of a more varied set of sight lines, including those toward background field stars as well as lower mass embedded protostars, may yet yield a detection of interstellar C_3O_2 , as, among other factors, the fraction of CO in the nonpolar (H_2O -poor) ice phase is higher in these colder environments (e.g., Chiar *et al.* 1995). Unfortunately, ISO observations toward the background field star Elias 16, which focused on detections of solid CO and CO_2 (Whittet *et al.* 1998), omitted the wavelength region containing the C_3O_2 ν_3 stretch because of time constraints imposed by the low flux level of this source.

There are also no positive detections of C_3O_2 toward comets (see, e.g., Irvine *et al.* 2000). This may be due to the fact that gas-phase C_3O_2 easily dissociates in the environment of cometary comae, as described in detail in Huntress *et al.* (1991). There is, however, reason to believe that comets may provide an environment capable of producing C_3O_2 . Comets contain large amounts of CO as a parent volatile in their nuclei, as evidenced by observations of the gases released in their comae (e.g., Irvine *et al.* 2000). This is not surprising, since comets are thought to have formed out of interstellar ices (either directly or indirectly) as the natal cloud condensed to form the young Sun. Highly volatile molecules such as CO may even be physically separated from

H_2O in the nuclei of short-period comets by heating and recooling during successive perihelion passages, resulting in a type of “cryogenic distillation.” The processing of such purer cometary CO ices by solar UV or galactic cosmic rays may lead to C_3O_2 in higher abundances than may be found in the interstellar medium. Based on our experiments, it is also likely that cometary C_3O_2 produced from energetic processing would remain intact in the nuclear ice or be converted by energetic processing to a dark polymeric residue. The large increase in the C_3O_2 vapor pressure from 110 to 125 K would imply that the release of C_3O_2 would increase greatly as the comet approached the Sun from a distance of about 7 to 5 AU. This increase in C_3O_2 would manifest itself as an increase in the amount of CO emission in the comet’s coma and the growth of an extended source of CO as the gas-phase C_3O_2 is dissociated. Of course, few comets are observed at such heliocentric distances because they are extremely faint, but emerging technologies, such as infrared interferometry or spaced-based telescopes, could make such observations possible.

APPENDIX: A COMMENT ABOUT THE REPORTING OF PRODUCT YIELDS

In this paper, we have presented initial formation and destruction yields for the products and reactants in our processing experiments. This is generally not the standard way of reporting radiolysis experiments, where a yield is reported after the application of a specified dose. For example, one might report that a certain number of molecules of product were created after a dose 100 eV, or that product’s yield, or “G value.” If a higher dose is applied, it is possible that the value of G reported (the number of products divided by total dose applied) will drop, as it represents the *yield averaged over the course of the entire irradiation*. This would most likely be due to the fact that the number of reactants is dropping while the number of products is rising, and the sample is approaching some sort of equilibrium chemistry (after which the reactant and product abundances remain constant). Such an example is shown in Fig. 5, where the average yield of C_3O_2 from CO is initially constant (as shown by the linear growth for doses less than about $2 \times 10^{19} eV cm^{-2}$) and later drops as the energy dose is further increased.

We have not reported the equilibrium constants here or the average formation rates of products but rather the rates of formation given by the zeroth- or first-order chemical reaction kinetics that take place when the energy applied interacts with the reactant molecules. This happens to be the standard way in which UV photolysis results are reported; see, e.g., Gerakines *et al.* (1996). UV formation and destruction rates are generally given in terms of cross sections as opposed to yields, but the two parameters provide the same information about the reactions and may be directly compared by a reasonably simple transformation of units (see discussion in Gerakines *et al.* 2000).

Initial formation rates, as opposed to the equilibrium rates, are given priority here because it is rare in an astrophysical context, given the typically small number of interactions per molecule or per unit time, to find a system *actually in chemical equilibrium*. Moreover, the simple mixtures we are studying (we have included only one or two components) do not by any means represent the complex ices found in space, but are merely models for the behavior of certain astrophysical ice components. It is therefore more appropriate here to study the low-order reaction kinetics, as they may be more easily implemented in chemical models where many more components may be included.

ACKNOWLEDGMENTS

We gratefully thank Reggie Hudson for a myriad of helpful discussions and good ideas. Steve Brown, Scott Kniffin and Claude Smith from NASA/GSFC’s Radiation Effects Facility are thanked for help with the irradiations. Alex Montoya from NASA/GSFC’s Materials Engineering Branch is thanked for

use of the FTIR microscope. This work was performed while P.A.G. held a NRC-NAS/NASA-GSFC research associateship.

REFERENCES

- Ames, L. L., D. White, and D. E. Mann 1963. Infrared absorption spectra of carbon suboxide and malononitrile in solid argon matrices. *J. Chem. Phys.* **38**, 910–917.
- Briggs, J. P., and P. G. Clay 1968. Formation of polymeric carbon suboxide during gamma radiolysis of liquid carbon monoxide at 77°K. *Nature* **218**, 355.
- Brodie, B. C. 1873. Note on the synthesis of marsh-gas and formic acid, and on the electric decomposition of carbonic oxide. *Proc. Roy. Soc. London* **21**, 245–247.
- Brucato, J. R., M. E. Palumbo, and G. Strazzulla 1997. Carbonic acid by ion implantation in water/carbon dioxide ice mixtures. *Icarus* **125**, 135–144.
- Chiar, J. E., A. J. Adamson, T. H. Kerr, and D. C. B. Whittet 1995. High-resolution studies of solid CO in the Taurus dark cloud: Characterizing the ices in quiescent clouds. *Astrophys. J.* **455**, 234–243.
- Dartois, E., W. Schutte, T. R. Geballe, K. Demyk, P. Ehrenfreund, and L. d'Hendecourt 1999. Methanol: The second most abundant ice species towards the high-mass protostars RAFGL7009S and W 33A. *Astron. Astrophys.* **342**, L32–L35.
- Eberhardt, P., D. Krankowsky, W. Schulte, P. Lämmerzahl, J. J. Berthelier, J. Woweries, U. Stubbemann, R. R. Hodges, J. H. Hoffman, and J. M. Illiano 1987. The CO and N₂ abundance in Comet P/Halley. *Astron. Astrophys.* **187**, 481–484.
- Elsila, J., L. J. Allamandola, and S. A. Sandford 1997. The 2140 cm⁻¹ (4.673 μm) solid CO band: The case for interstellar O₂ and N₂ and the photochemistry of nonpolar interstellar ice analogs. *Astrophys. J.* **479**, 818–838.
- Ewing, G. E., and G. C. Pimentel 1961. Infrared spectrum of solid carbon monoxide. *J. Chem. Phys.* **35**, 925–930.
- Festou, M. C., P. D. Feldman, M. F. A'Hearn, C. Arpigny, C. B. Cosmovici, A. C. Danks, L. A. McFadden, R. Gilmozzi, P. Patriarchi, G. P. Tozzi, M. K. Wallis, and H. A. Weaver 1986. IUE observations of Comet Halley during the VEGA and Giotto encounters. *Nature* **321**, 361–368.
- Gerakines, P. A., W. A. Schutte, J. M. Greenberg, and E. F. van Dishoeck 1995. The infrared band strengths of H₂O, CO, and CO₂ in laboratory simulations of astrophysical ice mixtures. *Astron. Astrophys.* **296**, 810–818.
- Gerakines, P. A., W. A. Schutte, and P. Ehrenfreund 1996. Ultraviolet processing of interstellar ice analogs. I. Pure ices. *Astron. Astrophys.* **312**, 289–305.
- Gerakines, P. A., D. C. B. Whittet, P. Ehrenfreund, A. C. A. Boogert, A. G. G. M. Tielens, W. A. Schutte, J. E. Chiar, E. F. van Dishoeck, T. Prusti, F. P. Helmich, and Th. de Graauw 1999. Observations of solid carbon dioxide in molecular clouds with the Infrared Space Observatory. *Astrophys. J.* **522**, 357–377.
- Gerakines, P. A., M. H. Moore, and R. L. Hudson 2000. Carbonic acid production in H₂O + CO₂ ices—UV photolysis vs. proton bombardment. *Astron. Astrophys.* **357**, 793–800.
- Gibb, E. L., D. C. B. Whittet, W. A. Schutte, A. C. A. Boogert, J. E. Chiar, P. Ehrenfreund, P. A. Gerakines, J. V. Keane, A. G. G. M. Tielens, E. F. van Dishoeck, and O. Kerkhof 2000. An inventory of interstellar ices toward the embedded protostar W33A. *Astrophys. J.* **536**, 347–356.
- Hagen, W., A. G. G. M. Tielens, and J. M. Greenberg 1983. A laboratory study of the infrared spectra of interstellar ices. *Astron. Astrophys. Suppl. Ser.* **51**, 389–416.
- Haring, R. A., R. Pedrys, D. J. Oostra, A. Haring, and A. E. de Vries 1984. Reactive sputtering of simple condensed gases by keV ions. II Mass spectra. *Nucl. Instrum. Methods. Phys. Res. B* **5**, 476–482.
- Hudson, R. L., and M. H. Moore 1995. Far-IR spectral changes accompanying proton irradiation of solids of astrochemical interest. *Radiat. Phys. Chem.* **45**, 779–789.
- Hudson, R. L., and M. H. Moore 1999. Laboratory studies of the formation of methanol and other organic molecules by water + carbon monoxide radiolysis: relevance to comets, icy satellites, and interstellar ices. *Icarus* **140**, 451–461.
- Huntress, W. T. Jr., M. Allen, and M. Delitsky 1991. Carbon suboxide in Comet Halley? *Nature* **352**, 316–318.
- Irvine, W. M., F. P. Schloerb, J. Crovisier, B. Fegley Jr., and M. J. Mumma 2000. Comets: A link between interstellar and nebular chemistry. In *Protostars and Planets IV* (V. Mannings, A. P. Boss, and S. S. Russell, Eds.), pp. 1159–1200. Univ. of Arizona Press, Tucson.
- Jiang, G. J., W. B. Person, and K. G. Brown 1975. Absolute infrared intensities and band shapes in pure solid CO and CO in some solid matrices. *J. Chem. Phys.* **64**, 1201–1211.
- Kouchi, A. 1987. Vapour pressure of amorphous H₂O ice and its astrophysical implications. *Nature* **330**, 550–552.
- Kranze, R. H., C. M. L. Rittby, and W. R. M. Graham 1996. Fourier transform infrared and theoretical isotopic study of the ν₄(σ_u) and ν₅(σ_u) modes of linear C₇. *J. Chem. Phys.* **105**, 5313–5320.
- Kuiper, G. P. 1957. The atmosphere and the cloud layer of Venus. In *The Threshold of Space* (M. Zelikoff, Ed.), pp. 85–86. Pergamon Press, New York.
- Kurtz, J., and D. R. Huffman 1990. Combined infrared and ultraviolet-visible spectroscopy of matrix-isolated carbon vapor. *J. Chem. Phys.* **92**, 30–35.
- Kybett, B. D., G. K. Johnson, C. K. Barker, and J. L. Margrave 1965. The heats of formatoin and polymerization of carbon suboxide. *J. Phys. Chem.* **69**, 3603–3606.
- Lind, S. C. 1928. *The Chemical Effects of Alpha Particles and Electrons*. Chemical Catalog Co, New York.
- McDougall, L. A., and J. E. Kilpatrick 1965. Entropy and related thermodynamic properties of carbon suboxide. *J. Chem. Phys.* **42**, 2311–2321.
- Miller, F. A., and W. G. Fateley 1964. The infrared spectrum of carbon suboxide. *Spectrochim. Acta* **20**, 253–266.
- Okabe, H. 1978. *Photochemistry of Small Molecules*. Wiley, New York.
- Pipes, J. G., J. A. Roux, A. M. Smith, and H. E. Scott 1978. Infrared transmission of contaminated cryocooled optical windows. *AIAA J.* **16**, 984–990.
- Plummer, W. T., and R. K. Carson 1970. Venus clouds: Test for carbon suboxide. *Astrophys. J.* **159**, 159–163.
- Sagdeev, R. Z., and 37 colleagues 1986. Television observations of Comet Halley from VEGA spacecraft. *Nature* **321**, 262–266.
- Sandford, S. A., L. J. Allamandola, A. G. G. M. Tielens, and G. J. Valero 1988. Laboratory studies of the infrared spectral properties of CO in astrophysical ices. *Astrophys. J.* **329**, 498–510.
- Smith, W. H., and G. E. Leroi 1966. Infrared and Raman spectra of carbon suboxide in condensed phases. *J. Chem. Phys.* **45**, 1767–1777.
- Sugimoto, S., M. Nishii, and T. Sugiura 1986. Radiation-induced chemical reactions of carbon monoxide and hydrogen mixture. 3. Solid materials produced under irradiation. *Radiat. Phys. Chem.* **27**, 147–151.
- Whittet, D. C. B., W. A. Schutte, A. G. G. M. Tielens, A. C. A. Boogert, Th. de Graauw, P. Ehrenfreund, P. A. Gerakines, F. P. Helmich, T. Prusti, and E. F. van Dishoeck 1996. An ISO-SWS view of interstellar ices: First results. *Astron. Astrophys.* **315**, L357–L360.
- Whittet, D. C. B., P. A. Gerakines, A. G. G. M. Tielens, A. J. Adamson, A. C. A. Boogert, J. E. Chiar, Th. de Graauw, P. Ehrenfreund, T. Prusti, W. A. Schutte, B. Vandenbussche, and E. F. van Dishoeck 1998. Detection of abundant CO₂ ice in the quiescent dark cloud medium toward Elias 16. *Astrophys. J.* **498**, L159–L163.
- Woods, T. N., P. D. Feldman, and K. F. Dymond 1987. The atomic carbon distribution in the coma of Comet P/Halley. *Astron. Astrophys.* **187**, 380–384.